mathematics

MDPI

Article

Impact of Parameter Variability and Environmental Noise on the Klausmeier Model of Vegetation Pattern Formation

Merlin C. Köhnke * and Horst Malchow

Institute of Environmental Systems Research, School of Mathematics, Computer Science, Osnabrück University, Barbarastraße 12, 49076 Osnabrück, Germany; horst.malchow@uos.de

* Correspondence: merlin.koehnke@uni-osnabrueck.de; Tel.: +49-541-969-2573

Received: 5 October 2017; Accepted: 14 November 2017; Published: 23 November 2017

Abstract: Semi-arid ecosystems made up of patterned vegetation, for instance, are thought to be highly sensitive. This highlights the importance of understanding the dynamics of the formation of vegetation patterns. The most renowned mathematical model describing such pattern formation consists of two partial differential equations and is often referred to as the Klausmeier model. This paper provides analytical and numerical investigations regarding the influence of different parameters, including the so-far not contemplated evaporation, on the long-term model results. Another focus is set on the influence of different initial conditions and on environmental noise, which has been added to the model. It is shown that patterning is beneficial for semi-arid ecosystems, that is, vegetation is present for a broader parameter range. Both parameter variability and environmental noise have only minor impacts on the model results. Increasing mortality has a high, nonlinear impact underlining the importance of further studies in order to gain a sufficient understanding allowing for suitable management strategies of this natural phenomenon.

Keywords: Klausmeier model; pattern formation; self-organization; reaction–diffusion–advection model; environmental noise

1. Introduction

Vegetation patterns have been observed in many semi-arid regions in Africa, Australia, North America, South America, and Asia [1]. They were first described in 1941 [2]. In the 1950s, the occurrence and the spatial distribution of these patterns were investigated on the basis of air photographs (e.g., [3]). It has been reported that periodic patterns at the border between semi-arid and arid climates are even omnipresent [4]. The diversity in patterns makes pattern formation in arid and semi-arid areas an interesting case study for pattern formation in ecology [5]. Furthermore, semi-arid regions are highly dynamic (e.g., [6]), which makes them an intriguing research area in general.

Different soil types supporting pattern formation exist, such as clay, sand and silt [7]. Various shapes of vegetation patterns, such as circles (e.g., [8]), spots (e.g., [9]), and stripes, arcs or labyrinths (e.g., [10]) where bare ground and vegetated bands alternate have been reported. The patterns can be formed by plants such as grass, shrubs or trees [11]. Observations showing transitions from anisotropic vegetation spots that elongate [12] to isotropic banded patterns with increasing slope exist (e.g., [11]). With decreasing precipitation, a successive transition from homogeneous vegetation over gaps, labyrinths and spots to a bare desert state has been observed [13]. The last step from vegetation spots to the bare desert state is commonly abrupt and is referred to as a catastrophic shift [14], which can be theoretically explained by the existence of two alternative stable states [15]. Recent studies suggest that this transition can be investigated on satellite images and can be used to retrieve information about imminent regime shifts [16]. The wavelength of banded patterns tends to decrease with increasing

slope and water input [7]. Some banded patterns show a slow uphill movement [17]. However, as a result of the slow speed, long-term data is necessary for reliable measurements. Usually, banded patterns form perpendicularly to the contour, but patterns parallel to the contour can also form under certain external impacts [18].

Early studies explain the formation of vegetation structures with the concept of islands of fertility (e.g., [19]). However, this does not give an appropriate explanation for the development [20]. More recent studies state that patterns emerge as a result of the coupling of reaction, diffusion and advection processes. Precipitation is not sufficient to ensure homogeneous vegetation in such areas. Thus, rainfall is the limiting factor of production [21], only allowing a bare desert state or patterned vegetation. The patterned vegetation facilitates the redistribution of the resource water [22] through diffusion and advection, yielding higher total plant biomass in comparison with homogeneous vegetation [23]. Furthermore, vegetation patterns can enhance accessibility of nutrients [24]. However, we note that different kinds of patterns can be observed within relatively small areas, which makes precipitation as the sole driving factor unlikely [20].

Different methods to model pattern formation and that describe this phenomenon by instabilities of uniform states exist [5]. Two common approaches are scale-dependent feedbacks (e.g., [25]) and competition for scarce resources (e.g., [26]). In the case of scale-dependent feedbacks, the range of facilitation must be shorter than the range of competition [11]. This is comparable to well-known systems with short-range activation and long-range inhibition in reaction–diffusion models [27,28]. In the case of vegetation pattern formation, the short-range activation can be given by increased soil permeability and shading of the plants, while the long-range activation can be given by growing roots competing for resources (e.g., [29]). However, we note that other approaches, such as stochastic models, explaining pattern formation as a consequence of noise-induced environmental fluctuations also exist (for a detailed review, see [1]). A large number of researchers have modelled the feedback between biomass growth and water use leading to pattern formation in semi-arid areas (e.g., [1,25,26,30,31]). More recent studies have also been focussing on the impact of heterogeneous environments [32] and heterogeneities in parameters [33] on pattern formation. They have pointed out that large patch sizes are a precondition for the widely considered self-organization [32].

Although many models describing pattern formation do already exist, the underlying mechanisms are still unclear. This article deals with the well-known reaction–diffusion–advection model by Klausmeier [30], which describes two-dimensional vegetation pattern formation as a function of the resource water. This model is commonly referred to as the Klausmeier model. It produces vegetation patterns that are banded if a gentle slope exists without any other environmental heterogeneities.

The aim of this study is to investigate whether variability or a change in different external conditions such as rainfall, evaporation or plant mortality has any influence on the system dynamics in a qualitative or in a quantitative manner. Here, the main focus is on the long-term dynamics of the model. To investigate the influence of variability in precipitation is particularly interesting, because constant rainfall is a strong assumption, as semi-arid areas are characterized by variable precipitation [34]. Periodicity can indeed have a strong influence on biomass dynamics [23]. Studies focussing on variability in precipitation already exist. However, the therein observed influence on the model behaviour is attributable either to model extensions of the Klausmeier model (e.g., [35]) or to a more detailed model structure (e.g., [36]). Therefore, it is interesting to investigate whether an influence on the classical Klausmeier model also exists. An investigation of the impact of changes in mean precipitation is particularly interesting because of its high influence on vegetation. However, it is still unclear how precipitation changes. Between 1955 and 2003, the total precipitation has been decreasing in western central Africa [37]. However, Leauthaud et al. [38] state that changes of -15% up to $+8\%$ in precipitation in semi-arid areas might be realistic depending on the scenario. Observations show that with high values of precipitation, a uniform plant distribution is reached, while at low values of precipitation, interactions between plants supporting self-organization are impossible because of the low biomass values [23]. Furthermore, the investigation of increasing mortality is justified as

human pressure on the vegetation due to land use tends to increase, which augments the risk of desertification [39]. Evaporation might change as a result of its dependency on temperature, which is why the investigation of the three parameters, precipitation, evaporation, and mortality, is important. The detailed investigations of the impact of various model parameters can be further compared with observations and can help to validate the structure of the model. Furthermore, it can help in understanding and ranking the possible influence of climate change and human impacts on semi-arid ecosystems in different stages of development as a result of the extensive parameter studies, which might provide information for a better-suited resource management.

This paper is structured as follows: Section 2 describes the Klausmeier model and analyses it regarding the existence and stability of equilibria. The numerical results are described in Section 3 and are discussed and interpreted in Section 4. Section 5 closes with a summary of the main conclusions.

2. Model and Methods

2.1. Model Description

The classical Klausmeier model consists of two coupled nonlinear partial differential equations representing water and biomass dynamics. It is described by Equation (1) with $A(T) = A$:

$$\frac{\partial N}{\partial T} = JRWN^2 - MN + D\Big(\frac{\partial^2}{\partial X^2} + \frac{\partial^2}{\partial Y^2}\Big)N \tag{1a}$$

$$\frac{\partial W}{\partial T} = A(T) - LW - RWN^2 + V\frac{\partial W}{\partial Y} \tag{1b}$$

The plants can grow on a two-dimensional domain with $(X, Y) \in \mathbb{R}^2$. Plant biomass grows through water uptake with a yield J. Plant mortality is given by MN. Furthermore, plants can spread through diffusion $D\Big(\frac{\partial^2}{\partial X^2} + \frac{\partial^2}{\partial Y^2}\Big)N$. The precipitation parameter $A(T)$ increases the amount of water W homogeneously in each grid cell. In the original model, precipitation is assumed to be constant (see [30]), while in this study, it can be time-dependent, as this is a strong characteristic feature in semi-arid areas [34]. The loss of water is divided into evaporation LW with a rate L and water uptake by plant biomass RWN^2. Water advection $V\frac{\partial W}{\partial Y}$ only takes place in the downhill direction.

For numerical investigations, the model has been nondimensionalized in two different ways (see Appendix A). The nondimensionalized model used for the investigation of the influence of the precipitation and the mortality is given by

$$\frac{\partial n}{\partial t} = wn^2 - mn + \Big(\frac{\partial^2}{\partial x^2} + \frac{\partial^2}{\partial y^2}\Big)n \tag{2a}$$

$$\frac{\partial w}{\partial t} = a(t) - w - wn^2 + v\frac{\partial w}{\partial y} \tag{2b}$$

The nondimensionalized model for the investigation of the influence of the evaporation is given by

$$\frac{\partial n}{\partial t} = wn^2 - mn + \Big(\frac{\partial^2}{\partial x^2} + \frac{\partial^2}{\partial y^2}\Big)n \tag{3a}$$

$$\frac{\partial w}{\partial t} = 1 - lw - wn^2 + v\frac{\partial w}{\partial y} \tag{3b}$$

To obtain shorter computing times and to facilitate interpretations, the one-dimensional model has been used in the analyses throughout this paper:

$$\frac{\partial n}{\partial t} = wn^2 - mn + \frac{\partial^2 n}{\partial y^2} \tag{4a}$$

$$\frac{\partial w}{\partial t} = 1 - lw - wn^2 + v\frac{\partial w}{\partial y} \tag{4b}$$

This means that plant diffusion only takes place parallel to the advection. To use the one-dimensional model is justified because the long-term behavior is considered and after sufficiently long simulation times, there does not exist any difference in the x-direction. This is due to the balancing effect of diffusion in the absence of a Turing instability.

2.2. Nonspatial Equilibria

The conditions for the spatially homogeneous equilibria are given by

$$\frac{\partial w}{\partial t} = a - w - wn^2 = 0 \tag{5a}$$

$$\frac{\partial n}{\partial t} = wn^2 - mn = 0 \tag{5b}$$

The semi-trivial solution $n_1^* = 0$ and $w_1^* = a$ corresponds to a completely bare state in a biological sense. The non-trivial solutions are given by

$$w_{2,3}^* = \frac{a}{2} \pm \sqrt{\frac{a^2}{4} - m^2} \tag{6a}$$

$$n_{2,3}^* = \frac{2m}{a \pm \sqrt{a^2 - 4m^2}} \tag{6b}$$

Imaginary solutions do not make biological sense here wherefore the square roots have to be positive. Figure 1 shows a bifurcation diagram of the system for the control parameter a.

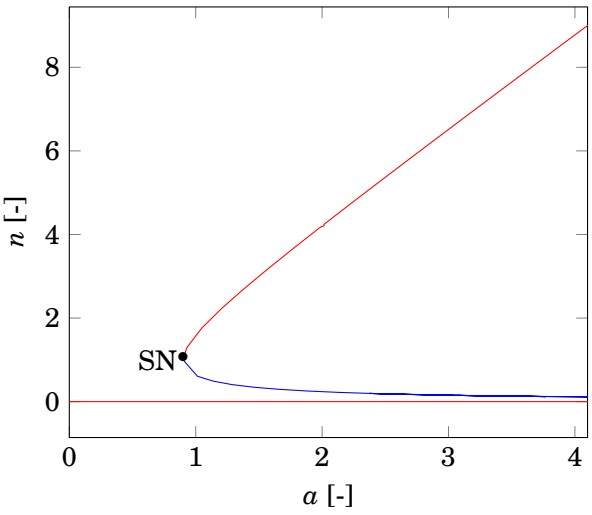

Figure 1. The bifurcation diagram for the control parameter a with $m = 0.45$ is shown. SN indicates the saddle-node bifurcation point. Red lines indicate stable equilibria, while the blue line indicates unstable equilibria.

The non-trivial equilibria only exist if $a \geq 2$ m, and $a = 2$ m corresponds to a saddle-node bifurcation point. In this case, only two equilibria exist. If $a < 2$ m, only the completely bare state

exists. Graphically, the reason for the vanishing of the non-trivial equilibria at low precipitation values lies in the flatter curve shape of the water nullcline with decreasing a (see Figure A1).

To investigate whether the equilibria are stable, the Jacobian matrix J is considered. The Jacobian is given by

$$J = \begin{pmatrix} -n_i^{*2} - 1 & -2w_i^* n_i^* \\ n_i^{*2} & 2w_i^* n_i^* - m \end{pmatrix} \tag{7}$$

For the semi-trivial equilibrium, the Jacobian reads

$$J_t = \begin{pmatrix} -1 & 0 \\ 0 & -m \end{pmatrix} \tag{8}$$

The eigenvalues of J_t are thus $\lambda_{J_t,1} = -1$ and $\lambda_{J_t,2} = -m$. As $m = ML^{-1}$ and $M > 0 \wedge L > 0$, both eigenvalues are real and negative. This means that the desert state is a stable node.

The eigenvalues of the non-trivial equilibria can be calculated by

$$\det \begin{pmatrix} -n_i^{*2} - 1 - \lambda & -2w_i^* n_i^* \\ n_i^{*2} & 2w_i^* n_i^* - m - \lambda \end{pmatrix} = 0 \tag{9}$$

With $w^* = \frac{m}{n^*}$, Equation (9) simplifies to

$$\det \begin{pmatrix} -n_i^{*2} - 1 - \lambda & -2m \\ n_i^{*2} & m - \lambda \end{pmatrix} = 0 \tag{10}$$

This leads to the eigenvalues

$$\lambda_\pm = -\frac{1}{2}(1 + n_i^{*2} - m) \pm \sqrt{m(1 - n_i^{*2}) + \frac{1}{4}(1 + n_i^{*2} - m)^2} \tag{11}$$

Stability can further be investigated using the approach from Siteur et al. [40]. Equation (11) has the form

$$\lambda_\pm = \alpha \pm \sqrt{\beta + \alpha^2} \tag{12}$$

Table 1 shows the real parts of the eigenvalues of the Jacobian for the form given by Equation (12).

Table 1. Real parts of the eigenvalues of the Jacobian as a function of α and β. λ_+ refers to the addition of the square root, while λ_- refers to the subtraction of the square root in Equation (12).

	$\beta > 0$	$\beta < 0$
$\alpha > 0$	$\mathrm{Re}(\lambda_+) > 0$ $\mathrm{Re}(\lambda_-) < 0$	$\mathrm{Re}(\lambda_+) > 0$ $\mathrm{Re}(\lambda_-) > 0$
$\alpha < 0$	$\mathrm{Re}(\lambda_+) > 0$ $\mathrm{Re}(\lambda_-) < 0$	$\mathrm{Re}(\lambda_+) < 0$ $\mathrm{Re}(\lambda_-) < 0$

Positive β always yields a node or a saddle point. The lower non-trivial equilibrium is a saddle point, as positive values of β always refer to real parts of the eigenvalues with different signs. This holds because Equation (13) is true for $m > 0$ and $a > 2$ m, which is already a condition for the existence of the non-trivial equilibria:

$$\beta = m\left[1 - \left(\frac{2m}{a + \sqrt{a^2 - 4m^2}}\right)^2\right] > 0 \tag{13}$$

If $\beta < 0$, the real parts of the eigenvalues will have the same signs. If they are negative, equilibria will be stable. Otherwise, equilibria will be unstable. Therefore, for stability of the larger equilibrium, Equations (14) and (15) must hold:

$$\beta = m\left[1 - \left(\frac{2m}{a - \sqrt{a^2 - 4m^2}}\right)^2\right] < 0 \tag{14}$$

$$\alpha = -\frac{1}{2}\left[1 + \left(\frac{2m}{a - \sqrt{a^2 - 4m^2}}\right)^2 - m\right] < 0 \tag{15}$$

β is negative if $m > 0$ and $a > 2$ m; α is negative if $0 < m \leq 1$ and $a \geq 2$ m. Because different values of m do not make biological sense, and because $a < 2$ m does not yield the existence of the non-trivial equilibrium, the higher non-trivial equilibrium is stable.

2.3. Differential Flow-Induced Instability

If diffusion exists in a system and the diffusion constants differ, a Turing instability can occur under certain circumstances (for a detailed review, see, e.g., [41]). In this system, diffusion only exists in the differential equation describing biomass dynamics. Hence, a Turing instability is not possible.

Besides diffusion, a differential flow exists in the model. This means that advection of biomass and advection of water differ, which can result in instabilities. In the following, this is investigated on the basis of the method described in Rovinsky and Menzinger [42].

Assuming small perturbations:

$$n(y,t) = n^* + n'(y,t) \tag{16a}$$

$$w(y,t) = w^* + w'(y,t) \tag{16b}$$

yields the following expressions for the one-dimensional model:

$$\frac{\partial n'}{\partial t} = 2wnn' + wn'^2 + w'n^2 + 2nw'n' + w'n'^2 - mn' + \frac{\partial^2 n'}{\partial y^2} \tag{17}$$

$$\frac{\partial w'}{\partial t} = -w' - wn^2 - 2wnn' - wn'^2 - w'n^2 - 2w'nn' - w'n'^2 + wn^2 + v\frac{\partial w'}{\partial y} \tag{18}$$

We note that the consideration of the one-dimensional model might overestimate the stability [43]. As we consider small perturbations, we can ignore terms that are nonlinear in terms of n' and w'. This leads to Equation (19) for the evolution of the perturbations:

$$\begin{pmatrix} \frac{\partial n'}{\partial t} \\ \frac{\partial w'}{\partial t} \end{pmatrix} = A \begin{pmatrix} n' \\ w' \end{pmatrix} + \begin{pmatrix} D & 0 \\ 0 & 0 \end{pmatrix} \begin{pmatrix} \frac{\partial^2 n'}{\partial y^2} \\ \frac{\partial^2 w'}{\partial y^2} \end{pmatrix} + \begin{pmatrix} 0 \\ v \end{pmatrix} \begin{pmatrix} \frac{\partial n'}{\partial y} \\ \frac{\partial w'}{\partial y} \end{pmatrix} \tag{19}$$

where A is the Jacobian evaluated at the steady state with $a_{i,j}$ being the entries of the matrix. Non-uniform perturbations that are exponential in time given by Equation (20) are applied:

$$n'(y,t) = e^{\lambda t + iky} \tag{20a}$$

$$w'(y,t) = e^{\lambda t + iky} \tag{20b}$$

with λ being the perturbation growth rate, k being the wavenumber, and i being the imaginary unit. Equation (21) is the eigenvalue equation:

$$\det(M) = \begin{vmatrix} a_{11} - Dk^2 - \lambda & a_{12} \\ a_{21} & a_{22} + ikv - \lambda \end{vmatrix} = 0 \tag{21}$$

The eigenvalues $\lambda_{\pm}$ are given by

$$\lambda_{\pm} = \frac{1}{2}\left(\mathrm{tr}(M) \pm \sqrt{\mathrm{tr}(M)^2 - 4\det(M)}\right) \tag{22}$$

with

$$\mathrm{tr}(M) = a_{11} + a_{22} - Dk^2 + \mathrm{i}kv \tag{23}$$

$$\det(M) = \det(A) - a_{22}Dk^2 + \mathrm{i}kv(a_{11} - Dk^2) \tag{24}$$

The saddle point is unstable against homogeneous perturbations and hence will not be further considered. To obtain instability in the non-trivial equilibrium, which is stable against homogeneous perturbations, the real part of one eigenvalue needs to be positive. This depends on the wavenumber k, on the slope v, on the mortality rate m and on the precipitation parameter a, which determine the stationary state. Figure 2 shows the dependence of the real part of the higher eigenvalue on these parameters.

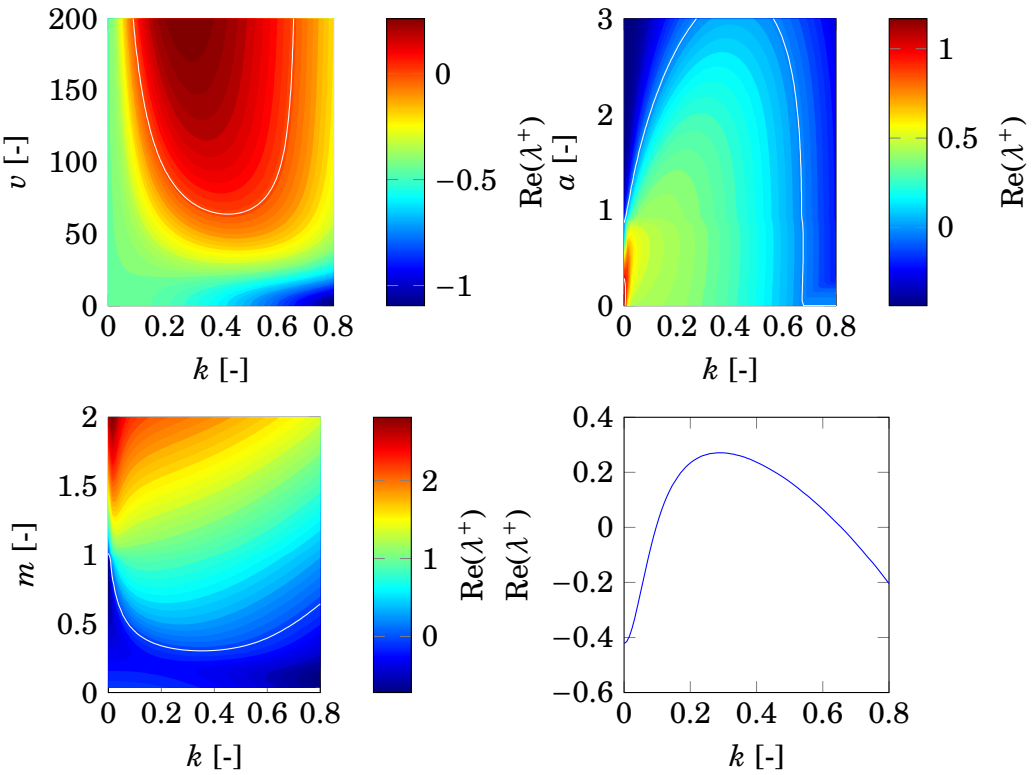

Figure 2. The dependence of the differential flow-induced instability on the wavenumber k, precipitation parameter a, slope v and mortality rate m is shown. Other parameters are given by the reference parameters for grass ($a = 2$, $m = 0.45$, and $v = 182.5$). The region of instability is restricted by the white line. The figure at the bottom right shows separately the dependence of the differential flow instability on the wavenumber for the reference values.

We note that the existence of the non-trivial equilibrium is restricted by $a \geq 2$ m. One can see that a differential flow-induced instability exists for the reference values. However, applying precipitation, slope and mortality values beyond a certain threshold leads to homogeneous vegetation.

The wavenumber corresponding to the maximum eigenvalue can be an indicator for the wavelength because it represents the fastest growing mode [44]. Hence, it can be seen that the wavelength tends to decrease with increasing precipitation and tends to increase with increasing

mortality. The influence of the slope is weaker. However, a small increase in wavelength occurs for increasing slope.

We note that complex eigenvalues result in traveling waves for which the velocity can be calculated [41]. This corresponds to the uphill migration in this model. However, the analytical investigation lies beyond the scope of this study. The interested reader may find further information regarding the analytical treatment of wavetrains in the Klausmeier model in Sherratt [45].

2.4. Considered Parameters

The nondimensionalized parameters a, m and l are considered for precipitation, mortality, and evaporation, respectively. In fact, these parameters depend on various ecological parameters. Nonetheless, they are proportional to their dimensioned counterparts. Hence, it is justified to use these parameters for the numerical investigations. The default values shown in Appendix B were used for all other parameters.

2.5. Precipitation Model

The function modeling variability in precipitation in this study is given by

$$a(t) = \max\left\{6.2832 \cdot \sin\left(\frac{2\pi t}{12} + \frac{2\pi}{12}\left(12 - 4.5\right)\right), 0\right\} \tag{25}$$

This should represent both the dry character of semi-arid areas and the periodicity in precipitation observed in many semi-arid regions, that is, monsoonal and mediterranean rain [23]. The data on which the precipitation model is based is shown in Appendix C. The factor 6.2832 is used to obtain a mean value of $a = 2$ to ensure comparability between the results with variable and constant precipitation. The maximum function is used to consider only the positive part of the sine function. This represents the semi-aridity.

2.6. Stochasticity

Besides including variability in precipitation, the addition of environmental noise to reduce the dependence of the model on initial conditions is analyzed in this study. This can be done by the following:

$$\frac{\partial n_i^j}{\partial t} - \frac{\partial^2 n_i^j}{\partial y^2} = f\left(n_i^j, w_i^j\right) + g\left(n_i^j\right)\eta_i^j \tag{26}$$

Here, n_i^j represents the value of the plant biomass at time-step i and cell j. The term η_i^j represents white noise distributed as a normal distribution with $\mathcal{N}(0,1)$; $g(n_i^j)$ represents the density-dependent noise intensity. This shrinks with increasing biomass, which can be justified by the assumption that low biomass is more prone to environmental fluctuations, while larger population sizes have a stabilizing effect [46]. The function that describes the density-dependent noise intensity is given by

$$g\left(n_i^j\right) = \mu \cdot 0.8^{n_i^j} \tag{27}$$

The choice of the function $g(n_i^j)$ is arbitrary to a certain extent. It is a trade-off between a function that is not too high at high biomass values to destroy the shape of the biomass peaks, on the one hand, and a function that is still high enough at lower biomass values to support the formation of a new biomass peak, on the other hand.

2.7. Numerical Treatment

We consider a one-dimensional domain $[0, L]$ with $\mathrm{d}x = 0.5$ and $L = 100/\mathrm{d}x$ representing 50 m in dimensional terms. As initial values, every grid cell has an amount of water $w_{ini} = 5$ and a biomass

that is given by a uniformly distributed random number in the interval [0.2, 0.4]. This is arbitrary to some degree. For the building up of biomass due to the positive biomass feedback loop, $n > 1$ is necessary in the first steps. This is achieved by the high initial water values but could also be achieved by random initial conditions with $n > 1$.

For the numerical solution of the model, the equations were discretized via the explicit Euler method with $h = 10^{-3}$ as the step size. The Forward-Time Central-Space (FTCS) explicit method has been used for diffusion and the Lax–Wendroff scheme has been used for advection. Periodic boundary conditions:

$$n(0) = n(L), \qquad n'(0) = n'(L) \tag{28}$$

$$w(0) = w(L), \qquad w'(0) = w'(L) \tag{29}$$

were used. This is biologically reasonable if one considers the grid as a particular section of the slope. For the numerical solution of the stochastic differential equation given by Eqaution (26), the Euler–Maruyama scheme has been applied (see [47]).

Unless otherwise stated, all data processing in this study was performed using Mat [48]. The data points for the uniform states in the bifurcation diagrams were calculated with the software XPPAUT [49]. Figures were drawn with Tikz [50].

3. Numerical Results

3.1. Precipitation

Figure 3 shows the impact of variations in variable and constant rainfall on existing vegetation patterns.

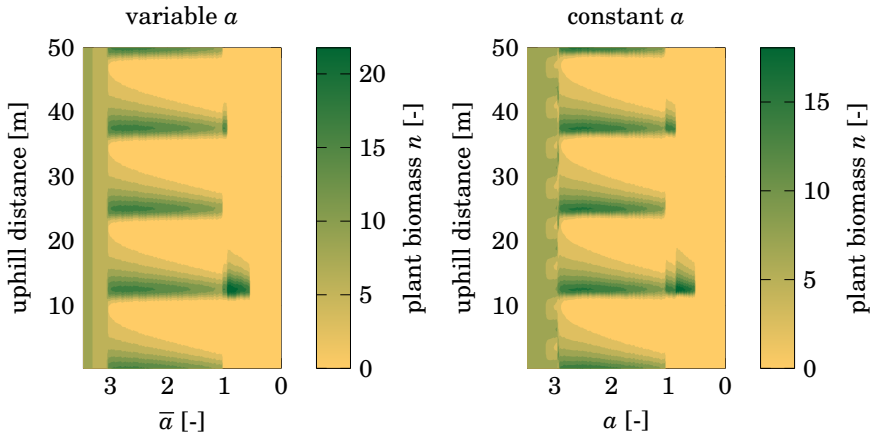

Figure 3. Results of the one-dimensional Klausmeier model after 1500 time-steps (to neglect transient dynamics) are shown for variable and constant precipitation. Resulting biomass peaks are shown for different values of mean precipitation. The maximum of plant biomass is located at 12.5 m uphill distance for each run to facilitate comparison and interpretation. As initial conditions, four peaks resulting from a model run with $\overline{a} = 2$ have been used.

In both cases, the system is in a state with four peaks (initial state) for a broad parameter range. In the case of variable precipitation, a critical precipitation value exists at which the four peaks vanish and homogeneous vegetation emerges. On the contrary, the system with constant precipitation shows a period doubling before homogeneous vegetation emerges. Considering lower parameter values of a, period halving in both cases can be observed. The critical values at which the period halving occurs are slightly different however. Furthermore, a critical value exists beyond which the bare desert state emerges.

Figure 4 shows the dependence of biomass patterns on the precipitation with constant random initial conditions.

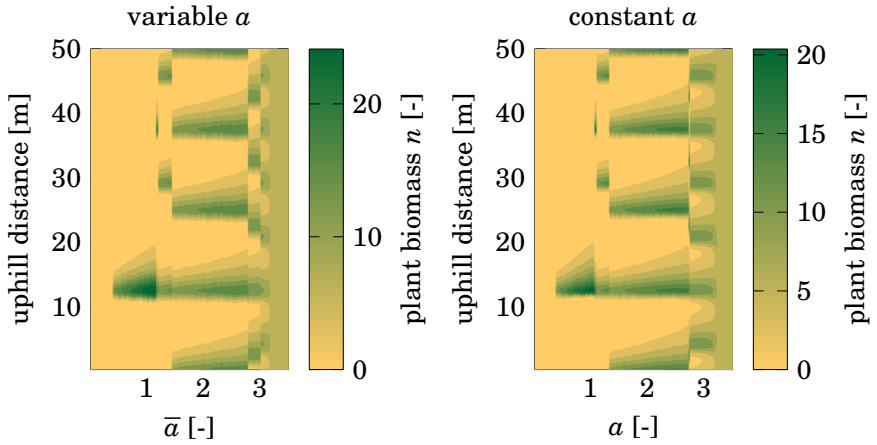

Figure 4. Results of the one-dimensional Klausmeier model after 1500 time-steps are shown for variable and constant precipitation. Resulting biomass peaks are shown for different values of mean precipitation. The maximum of plant biomass is located at 12.5 m uphill distance for each run. Random initial conditions have been used. Initial conditions have been the same for every value of $\overline{a}$.

In contrast to Figure 3, period doubling cannot be observed. Higher values of $\overline{a}$ lead to successive increases in the number of maxima in plant biomass. The parameter ranges in which certain numbers of peaks occur differ from those of Figure 3. However, four peaks are still the preferred state of the system. Variable and constant precipitation show the same general behavior. Nevertheless, the exact values at which certain numbers of maxima occur differ.

3.2. Stochasticity

To reduce the influence of the initial conditions on the wavenumber, stochasticity can be added to the model. We note that various numerical investigations have been made for different stochastic terms and for variable and constant precipitation. However, there have been no qualitative differences in the results of the model.

Figure 5 shows the long-term results of the one-dimensional model for different values of a and random initial conditions.

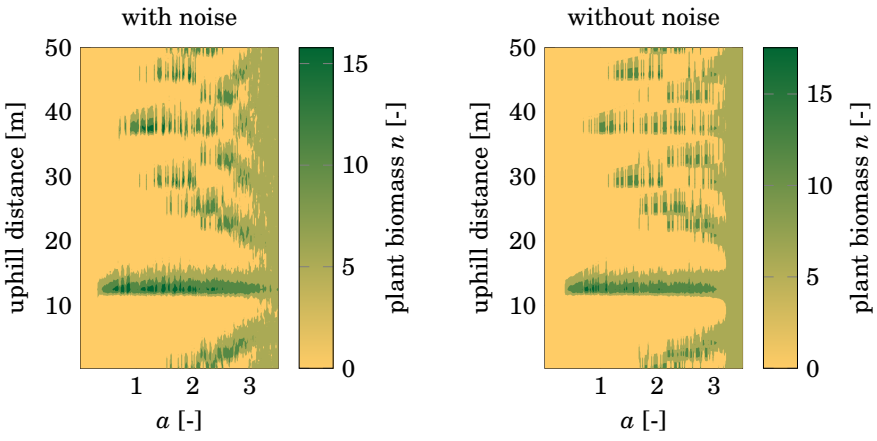

Figure 5. Results of the one-dimensional Klausmeier model after 1500 time-steps are shown for constant precipitation. Resulting biomass peaks are shown for different values of the parameter a. The maximum of plant biomass is located at 12.5 m uphill distance for each run. Varying random initial conditions have been used. For the generation of the left plot, the stochastic differential equation given by Equation (26) has been used for calculation of the plant biomass.

Clearly, there is no qualitative difference between the results of the model with noise and the results of the model without noise in terms of the wavenumber. Both cases show varying wavenumbers for different initial conditions. However, there are some parameter regions in which the model with noise leads to different wavenumbers in comparison with the model without noise.

3.3. Effect of Pattern Formation

As a result of the patterned vegetation, precipitation can be significantly lower while mortality and evaporation can be significantly higher before yielding the bare desert state. This is illustrated in the bifurcation diagrams in Figure 6.

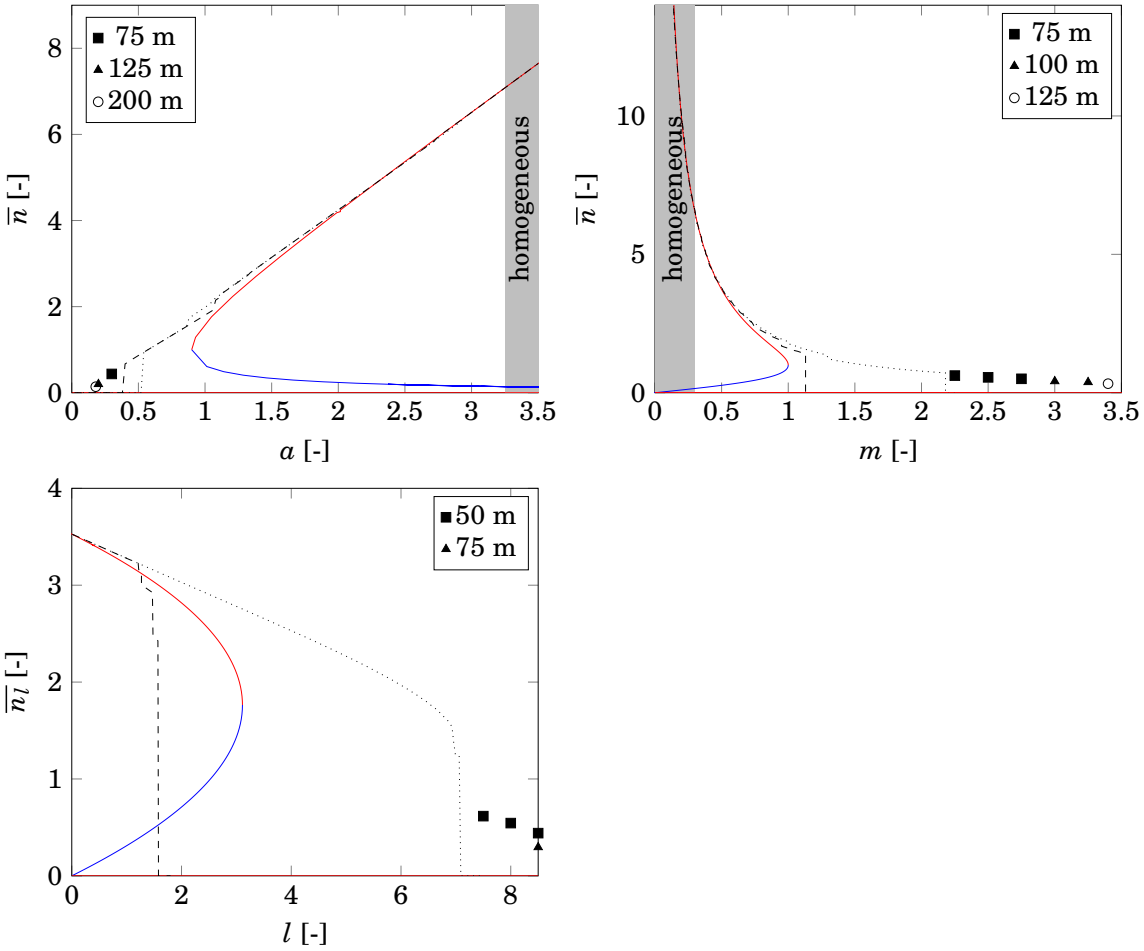

Figure 6. Bifurcation diagrams for different control parameters are shown. Red lines indicate stable equilibria, while the blue lines indicate unstable equilibria. The dashed line indicates the mean biomass with random initial conditions, while the dotted line indicates the mean biomass with four peaks as initial conditions. The square, the triangle, and the circle indicate the mean biomass for lower values of precipitation and higher values of mortality or evaporation with larger domain size and one biomass peak as initial conditions.

The biomass of the patterned state is in the same order of magnitude as the biomass of the uniform equilibrium in all cases. Furthermore, one can see that the wavenumber and hence the shift to the bare desert state depend on the size of the domain.

Below $a \approx 0.18$, the bare desert state is always reached, independent of the domain size and the initial conditions.

The transition to the bare desert state takes place at a significantly higher mortality in the case of existing patterns as initial conditions. The lowest value leading to pattern formation and the lowest

value preserving an existing pattern differ by a factor of approximately 2 for a domain size of 50 m. Applying larger domain sizes enhances the parameter range yielding patterns for the case of one peak as initial conditions until approximately $m = 3.4$. Larger domain sizes have no effect in the case of random initial conditions yielding a factor of 3.1.

The lowest value of the evaporation rate leading to pattern formation differs from the lowest value preserving an existing pattern by a factor of 4.5. Applying only one peak as initial conditions yields a factor of 5.4. However, in the case of lower wavenumbers or larger domains, the mean biomass decreases sharply.

4. Discussion

4.1. Influence of Variable Precipitation

The formation of vegetation patterns can be achieved by variable and constant precipitation with some minor quantitative differences. Thus, parameter variability has only limited impacts on the model behavior in the case of precipitation.

The existing pattern as initial conditions persists over a broad parameter range. This supports the prevailing view of the necessity of improved environmental conditions for the reverse transition (e.g., [5]). The lowest precipitation value leading to pattern formation and the lowest precipitation value preserving existing patterns differ by a factor of 0.7 and are thus in accordance with the factor provided by Sherratt and Lord [51]. This can be explained as follows. In the case of random initial conditions, the strongest initial perturbation builds up to a biomass peak. In the case of existing patterns as initial conditions, the disturbances are very small. Thus, the strongest perturbation cannot build up quickly enough. If $n_{max} < 1$, the quadratic biomass term does not lead to fast biomass growth. Hence, the major perturbation has to be large enough to support a single biomass peak before the biomass drops under a critical value. This is not the case for random initial conditions.

Starting with random initial conditions, higher wavenumbers can occur in the case of constant precipitation. This can be explained as follows. Let a weak disturbance in plant biomass exist. In the case of variable precipitation, the year starts with a drought period. This can lead to biomass near to extinction before the rainy season begins. Conversely, in the case of constant precipitation, no drought period exists. Therefore, the biomass disturbance can lead to a biomass peak. This means that the initial biomass n must have a value that supports biomass growth with the given amount of water. Mathematically, this can be obtained by Equation (30) in the case of constant precipitation, keeping in mind that $n \geq 0$:

$$wn^2 - mn > 0 \longrightarrow wn > m \tag{30}$$

Furthermore, biomass needs to be sufficiently small so as not to build up enough in the rainy season. This means that Equation (31) must hold in the case of variable precipitation:

$$wn - m\Big|_{\text{rainy}} < m - wn\Big|_{\text{drought}} \tag{31}$$

As $w > m$ in the rainy season, this implies that the initial drought must lead to $n \ll 1$. The critical value depends on the length of the rainy season and precipitation in the rainy season.

We note that the influence of drought periods has also been investigated. However, the resulting figures are not of major significance; thus, they are not shown in this paper. Applying an already established pattern as initial conditions, the system remains in this state without changing the wavenumber unless the drought period leads to extinction.

4.2. Dependence on Initial Conditions

Applying varying random initial conditions for the same precipitation value, a strong dependence of the system behavior on the initial conditions became evident. An explanation for this dependence

could be that two prerequisites for the formation of a biomass peak exist. First, a disturbance in biomass is needed so that biomass can build up. Second, a sufficiently large amount of water is required. Because in Figure 5 different initial conditions for each value of a have been applied, disturbances in biomass differ. If the amount of water in the system is large enough to support a specific wavenumber but no disturbance large enough and remote enough from the neighboring disturbance exist, biomass cannot build up. To overcome this shortcoming of the one-dimensional model, a stochastic term representing environmental noise has been added. This shows only a weak influence. On the one hand, the fact that multiplicative noise with zero mean has been used ensures that biomass cannot become negative and the noise does not add biomass to the system. On the other hand, this results in the fact that the effect is a maximum in regions with high biomass. Negative noise effects in those regions do not change the long-term behavior, because the diffusion of the neighbored cells is too high. Conversely, in the regions with low biomass, in which new biomass peaks should build up if precipitation is high enough to ensure a higher wavenumber, the effect of the noise is very small. Thus no peak can build up. Hence, the stochastic term is not suited to overcome the shortcoming of the dependence on the initial conditions.

4.3. Comparison with Nonspatial Equilibria

In comparison with the nonspatial equilibria, patterns are beneficial for the ecosystem. However, a lower bound of precipitation exists, beyond which the bare desert state is always reached. This is in accordance with Sherratt and Lord [51]. The reason for this lower bound is that, as a result of the evaporation, the upper bound on the amount of water on a grid cell is a, which is independent of the biomass.

In the case of random initial conditions and increasing mortality, larger domain sizes have no effect on the parameter range allowing for vegetation patterns (see Figure 6). This is opposite to the effect of precipitation and can be explained as follows. The precipitation parameter increases the amount of water in the system. For $n < 1$, the effect of a change in precipitation is low because of the multiplication with the square of the biomass. This is the case for the random initial conditions applied in this study. On the other hand, the mortality only depends on the biomass, which is not squared. For $n > 1$, the square of the biomass yields a higher effect of the change of precipitation in comparison to the mortality rate. This is the case for already formed patterns as initial conditions.

The application of higher evaporation rates is the only case in which a sharp decrease in plant biomass can be observed. The system remains in its initial state for a broad parameter range. This occurs because the influence of the evaporation rate depends on the amount of water, with $w_l \ll 1$ at the biomass peak. Furthermore, the change in the amount of water depends on the water uptake by plants, which in turn depends on the square of biomass. Changes in evaporation only have a small influence on the system, because $n_l^2 \gg l$. However, the peak cannot benefit from larger domain sizes because only water from imminent grid cells reaches the biomass peak. Water from remote cells is lost as a result of the evaporation.

The case of increasing evaporation and random initial conditions applied is the only case of all the analyses leading to extinction before the bifurcation point. This occurs because the evaporation rate at the bifurcation point is beyond 1. With random initial conditions applied, $n_l < 1$ holds for the first time-steps. Thus, biomass cannot build up effectively. Therefore, a large amount of water is needed to ensure the emergence of biomass peaks. If we apply $w_l = 5$ as initial values of water, the evaporation rate has a high impact. Hence, if $l \geq 1$, it makes the building up of the biomass unlikely. The exact value depends on the initial conditions, because these determine how fast a biomass peak can build up. If $n > 1$ and $w < 1$ would have been applied as initial conditions, the influence of the evaporation on the emergence of patterns would likely be significantly lower. We note that even at lower evaporation rates, the system would not reach the non-trivial equilibrium but would be attracted to the bare desert state. Hence, vegetation patterns are still beneficial in comparison with the uniform states.

In the case of decreasing precipitation or increasing mortality, a decrease in the wavenumber occurs via period halvings, which might explain regime shifts observed in reality. This will occur if the amount of water is not sufficient to ensure the present wavenumber. We note that small deviations are necessary. First, the amplitude of the four initial biomass peaks decreases as a result of the lack of water. Driven by the small deviation, one biomass peak can take up more water. This, in turn, leads to an even greater lack of water at the following peak, which consequently shrinks and gives an advantage to the next peak.

5. Conclusions

Variable precipitation has only minor impacts on the qualitative system behavior. It is doubtful whether the findings of the impact of variable precipitation make sense in a biological way. Because pattern formation in semi-arid areas is difficult to observe (e.g., caused by long time-scales), this cannot be supported by data. Moreover, we note that variability in precipitation has more complex influences on surface runoff (e.g., an increase due to saturated soils). These are not considered in the model.

A high influence of the mortality on the patterns also exists. Increasing the mortality rate (as is done, e.g., by wood cutting) can lead to severe changes in the vegetation pattern and in the total plant biomass in this model. The impact of the mortality rate on the total plant biomass is highly nonlinear. This underlines the importance of taking the mortality in analyses into account, as the biomass is crucial for populations depending on these resources.

To the authors' best knowledge, this study is the first taking the influence of the evaporation on the Klausmeier model or other models describing pattern formation into account. The reason might be that the prediction of changes in evaporation is very complex. Nevertheless, water as the limiting resource in semi-arid areas is closely linked to evaporation, justifying detailed investigations. However, as evaporation is proportional to the amount of water and $w_l \ll 1$ in the model, the effect of the evaporation rate is relatively low in the model.

In all investigations, a strong dependence on the initial conditions became evident. In particular, the preferred wavenumbers not only depended on initial conditions but also on the history (see also Sherratt and Lord [51]) in some cases. An attempt to reduce the dependence of the wavenumber on initial conditions has been presented. This did not succeed because of the density-dependence of the noise.

In all analyses, except in the case of increasing evaporation, patterns enhanced the parameter region for vegetation beyond the bifurcation point. This indicates the benefit of vegetation patterns for semi-arid ecosystems. It has been shown that the exact parameter regions can depend on the grid size.

Acknowledgments: The authors appreciated Matthew W. Adamson's critical reading of the manuscript. Furthermore, they are thankful for the comments of two anonymous referees.

Author Contributions: The results are part of Merlin C. Köhnke's Master's thesis under Horst Malchow's supervision.

Conflicts of Interest: The authors declare no conflict of interest.

Appendix A. Nondimensionalization

Appendix A.1. Nondimensionalization in Terms of Precipitation and Mortality

The classical Klausmeier model with physical parameters is given by Equation (A1) with $A(T) = A$:

$$\frac{\partial N}{\partial T} = JRWN^2 - MN + D\left(\frac{\partial^2}{\partial X^2} + \frac{\partial^2}{\partial Y^2}\right)N \tag{A1a}$$

$$\frac{\partial W}{\partial T} = A(T) - LW - RWN^2 + V\frac{\partial W}{\partial Y} \tag{A1b}$$

For nondimensionalization, constant values with the same physical units as the corresponding physical parameters are chosen. It follows that the ratio is dimensionless. Inserting the values

$$N = nN_0, \quad W = wW_0, \quad T = tT_0, \quad X = xX_0, \quad Y = yY_0$$

yields

$$\frac{\partial n}{\partial t} = JRwW_0n^2N_0T_0 - MnT_0 + D\left(\frac{\partial^2}{\partial x^2} + \frac{\partial^2}{\partial y^2}\right)n\frac{T_0}{X_0Y_0} \tag{A2a}$$

$$\frac{\partial w}{\partial t} = A(T)\frac{T_0}{W_0} - LwT_0 - RwT_0n^2N_0^2 + V\frac{T_0}{Y_0}\frac{\partial w}{\partial y} \tag{A2b}$$

In order to simplify the equations, the following are assumed:

$$\begin{aligned}
LT_0 = 1 &\rightarrow T_0 = L^{-1},\\
RT_0N_0^2 = 1 &\rightarrow N_0 = L^{\frac{1}{2}}R^{-\frac{1}{2}}\\
JRW_0T_0N_0 = 1 &\rightarrow W_0 = J^{-1}L^{\frac{1}{2}}R^{-\frac{1}{2}}\\
DT_0X_0^{-1}Y_0^{-1} = 1 &\xrightarrow{X=Y} X_0 = Y_0 = L^{-\frac{1}{2}}D^{\frac{1}{2}}\\
a(t) = A(T)T_0W_0^{-1} &\rightarrow a(t) = A(T)JL^{-\frac{3}{2}}R^{\frac{1}{2}}
\end{aligned}$$

As every constant value is defined, we obtain the following nondimensionalized parameters:

$$\begin{aligned}
t &= LT,\\
n &= NL^{-\frac{1}{2}}R^{\frac{1}{2}}\\
w &= WJL^{-\frac{1}{2}}R^{\frac{1}{2}}\\
x &= XL^{\frac{1}{2}}D^{-\frac{1}{2}}\\
y &= YL^{\frac{1}{2}}D^{-\frac{1}{2}}\\
v &= VT_0Y_0^{-1} \rightarrow v = VL^{-\frac{1}{2}}D^{-\frac{1}{2}}\\
m &= MT_0 \rightarrow m = ML^{-1}
\end{aligned}$$

Using these parameters yields the nondimensionalized form given by Equation (A3):

$$\frac{\partial n}{\partial t} = wn^2 - mn + \left(\frac{\partial^2}{\partial x^2} + \frac{\partial^2}{\partial y^2}\right)n \tag{A3a}$$

$$\frac{\partial w}{\partial t} = a(t) - w - wn^2 + v\frac{\partial w}{\partial y} \tag{A3b}$$

We note that this form only has the three parameters $a(t)$, v and m.
Figure A1 shows the nullclines of the system for different values of a.

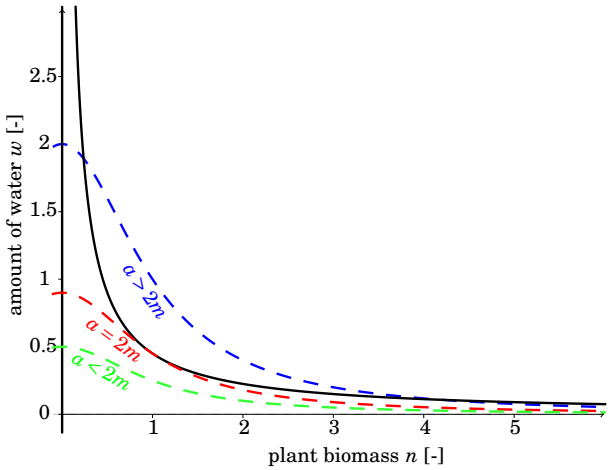

Figure A1. The nullclines of the nondimensionalized nonspatial system (see Equation (5)) are shown. Dashed lines represent the water nullclines, while the solid lines represent the biomass nullclines. Note that one solid line is represented by the ordinate.

Appendix A.2. Nondimensionalization in Terms of Evaporation

To investigate the influence of the evaporation on the system, another nondimensionalization has been taken. The first step is the same as in Appendix A.1, which again yields Equation (A2).

For simplification, the following are assumed:

$$\begin{aligned} RT_0N_0^2 &= 1 \\ T_0JRW_0N_0 &= 1 \\ T_0X_0^{-1}Y_0^{-1}D &= 1 \\ T_0AW_0^{-1} &= 1 \end{aligned}$$

Combining these assumptions, one obtains the following expressions for the constants:

$$\begin{aligned} T_0 &= A^{-\frac{2}{3}}J^{-\frac{2}{3}}R^{-\frac{1}{3}} \\ N_0 &= A^{\frac{1}{3}}J^{\frac{1}{3}}R^{-\frac{1}{3}} \\ W_0 &= A^{\frac{1}{3}}J^{-\frac{2}{3}}R^{-\frac{1}{3}} \\ Y_0 &= X_0 = D^{\frac{1}{2}}A^{-\frac{1}{3}}J^{-\frac{1}{3}}R^{-\frac{1}{6}} \end{aligned}$$

This yields the following nondimensionalized parameters:

$$\begin{aligned} t &= TA^{\frac{2}{3}}J^{\frac{2}{3}}R^{\frac{1}{3}} \\ n &= NA^{-\frac{1}{3}}J^{-\frac{1}{3}}R^{\frac{1}{3}} \\ w &= WA^{-\frac{1}{3}}J^{\frac{2}{3}}R^{\frac{1}{3}} \\ x &= XD^{-\frac{1}{2}}A^{\frac{1}{3}}J^{\frac{1}{3}}R^{\frac{1}{6}} \\ y &= YD^{-\frac{1}{2}}A^{\frac{1}{3}}J^{\frac{1}{3}}R^{\frac{1}{6}} \\ l &= LA^{-\frac{2}{3}}J^{-\frac{2}{3}}R^{-\frac{1}{3}} \\ v &= VA^{-\frac{1}{3}}D^{-\frac{1}{2}}J^{-\frac{1}{3}}R^{-\frac{1}{6}} \\ m &= MA^{-\frac{2}{3}}J^{-\frac{2}{3}}R^{-\frac{1}{3}} \end{aligned}$$

Using these parameters, the nondimensionalized form to investigate the influence of the evaporation is given by Equation (A4):

$$\frac{\partial n}{\partial t} = wn^2 - mn + \left(\frac{\partial^2}{\partial x^2} + \frac{\partial^2}{\partial y^2}\right) n \tag{A4a}$$

$$\frac{\partial w}{\partial t} = 1 - lw - wn^2 + v\frac{\partial w}{\partial y} \tag{A4b}$$

Appendix B. Default Values

The default values for the physical parameters for grass given by Klausmeier [30] are shown in Table A1.

We note that $V \gg D$, because even on gentle slopes, the advection of water is assumed to be much faster than the plant dispersal.

Table A1. Physical parameters and their default values and units are shown for grass. The values are taken from Klausmeier [30].

Physical Parameter	Value	Unit
T		a
W		kg m^{-2}
N		kg m^{-2}
X		m
Y		m
A	533	kg m^{-2} a^{-1}
L	4	a^{-1}
R	100	m^{-2} kg^{-2} a^{-1}
J	0.003	—
V	365	m a^{-1}
M	1.8	a^{-1}
D	1	m^2 a^{-1}

Appendix C. Precipitation Model

Figure A2 shows the average precipitation in Niamey, Niger for the period 1961–1990, with the corresponding function used to model variability in precipitation.

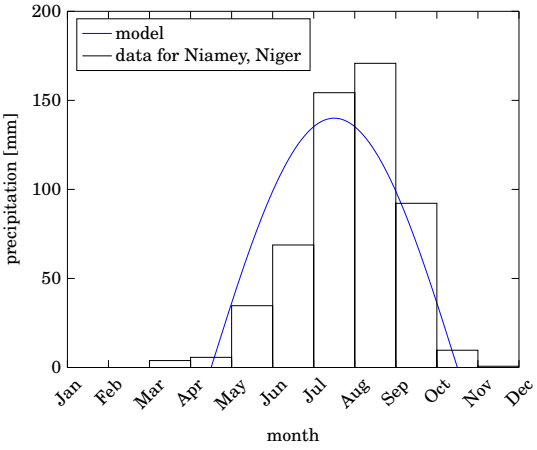

Figure A2. Average precipitation for Niamey, Niger (1961–1990) and the corresponding model are shown. Precipitation data retrieved from [52]. The geographic position of the station is N13°29′, E2°10′.

The region was chosen because it is a semi-arid region with good data coverage, where vegetation structures can be observed. The average annual precipitation in this region is 540.8 mm [52]. It can be seen that most rainfall occurs between May and September. In the remaining months, there are very low levels of rainfall. This is typical for semi-arid areas and justifies an investigation of the influence of such a variability on the results of the model.

References

1. Borgogno, F.; D'Odorico, P.; Laio, F.; Ridolfi, L. Mathematical models of vegetation pattern formation in ecohydrology. *Rev. Geophys.* **2009**, *47*, RG1005, doi:10.1029/2007RG000256.
2. Gillett, J. The plant formations of western British Somaliland and the Harar province of Abyssinia. *Misc. Bull. Inf.* **1941**, *1941*, 35–75.
3. Macfadyen, W.A. Vegetation patterns in the semi-desert plains of British Somaliland. *Geogr. J.* **1950**, *116*, 199–211.
4. Deblauwe, V.; Barbier, N.; Couteron, P.; Lejeune, O.; Bogaert, J. The global biogeography of semi-arid periodic vegetation patterns. *Glob. Ecol. Biogeogr.* **2008**, *17*, 715–723.
5. Meron, E. *Nonlinear Physics of Ecosystems*, 1st ed.; CRC Press: Boca Raton, FL, USA, 2015.
6. Gibbens, R.; McNeely, R.; Havstad, K.; Beck, R.; Nolen, B. Vegetation changes in the Jornada Basin from 1858 to 1998. *J. Arid Environ.* **2005**, *61*, 651–668.
7. Tongway, D.J.; Valentin, C.; Seghieri, J. (Eds.) *Banded Vegetation Patterning in Arid and Semiarid Environments*; Springer: New York, NY, USA, 2001.
8. Juergens, N. The biological underpinnings of Namib desert fairy circles. *Science* **2013**, *339*, 1618–1621.
9. Bromley, J.; Brouwer, J.; Barker, A.; Gaze, S.; Valentine, C. The role of surface water redistribution in an area of patterned vegetation in a semi-arid environment, south-west Niger. *J. Hydrol.* **1997**, *198*, 1–29.
10. White, L.P. Vegetation stripes on sheet wash surfaces. *J. Ecol.* **1971**, *59*, 615–622.
11. Barbier, N.; Couteron, P.; Lejoy, J.; Deblauwe, V.; Lejeune, O. Self-organized vegetation patterning as a fingerprint of climate and human impact on semi-arid ecosystems. *J. Ecol.* **2006**, *94*, 537–547.
12. Couteron, P.; Lejeune, O. Periodic spotted patterns in semi-arid vegetation explained by a propagation-inhibition model. *J. Ecol.* **2001**, *89*, 616–628.
13. Deblauwe, V.; Couteron, P.; Lejeune, O.; Bogaert, J.; Barbier, N. Environmental modulation of self-organized periodic vegetation patterns in Sudan. *Ecography* **2011**, *34*, 990–1001.
14. Scheffer, M.; Carpenter, S.; Foley, J.A.; Folke, C.; Walker, B. Catastrophic shifts in ecosystems. *Nature* **2001**, *413*, 591–596.
15. Scheffer, M.; Carpenter, S.R. Catastrophic regime shifts in ecosystems: Linking theory to observation. *Trends Ecol. Evol.* **2003**, *18*, 648–656.
16. Mander, L.; Dekker, S.C.; Li, M.; Mio, W.; Punyasena, S.W.; Lenton, T.M. A morphometric analysis of vegetation patterns in dryland ecosystems. *R. Soc. Open Sci.* **2017**, *4*, 160443.
17. Montana, C. The colonization of bare areas in two phase mosaics of an arid ecosystem. *J. Ecol.* **1992**, *80*, 315–327.
18. Maestre, F.T.; Reynolds, J.F.; Huber-Sannwald, E.; Herrick, J.; Smith, M.S. Understanding global desertification: Biophysical And socioeconomic dimensions of hydrology. In *Dryland Ecohydrology*; D'Odorico, P., Porporato, A., Eds.; Springer: Dordrecht, The Netherlands, 2006; pp. 315–332.
19. Charley, J.L.; West, N.E. Plant-induced soil chemical patterns in some shrub-dominated semi-desert ecosystems of Utah. *J. Ecol.* **1975**, *63*, 945–963.
20. Stewart, J.; Parsons, A.J.; Wainwright, J.; Okin, G.S.; Bestelmeyer, B.T.; Fredrickson, E.L.; Schlesinger, W.H. Modeling emergent patterns of dynamic desert ecosystems. *Ecol. Monogr.* **2014**, *84*, 373–410.
21. Dudney, J.; Hallett, L.M.; Larios, L.; Farrer, E.C.; Spotswood, E.N.; Stein, C.; Suding, K.N. Lagging behind: Have we overlooked previous-year rainfall effects in annual grasslands? *J. Ecol.* **2016**, *105*, 484–495.
22. Bergkamp, G.; Cammeraat, L.H.; Martinez-Fernandez, J. Water movement and vegetation patterns on shrubland and an abandoned field in two desertification-threatened areas in Spain. *Earth Surf. Proc. Land.* **1996**, *21*, 1073–1090.
23. Noy-Meir, I. Desert ecosystems: Environment and producers. *Annu. Rev. Ecol. Syst.* **1973**, *4*, 25–51.
24. Schlesinger, W.H.; Raikes, J.A.; Hartley, A.E.; Cross, A.F. On the spatial pattern of soil nutrients in desert ecosystems. *Ecology* **1995**, *77*, 364–374.
25. Lefever, R.; Lejeune, O. On the origin of tiger bush. *Bull. Math. Biol.* **1997**, *59*, 263–294.
26. von Hardenberg, J.; Meron, E.; Shachak, M.; Zarmi, Y. Diversity of vegetation patterns and desertification. *Phys. Rev. Lett.* **2001**, *87*, 198101.
27. Nicolis, G.; Prigogine, I. *Self-Organization in Nonequilibrium Systems: From Dissipative Structures to Order Through Fluctuations*; Wiley: New York, NY, USA, 1977.
28. Gierer, A.; Meinhardt, H. A theory of biological pattern formation. *Kybernetik* **1972**, *12*, 30–39.

29. Lefever, R.; Barbier, N.; Couteron, P.; Lejeune, O. Deeply gapped vegetation patterns: On crown/root allometry, criticality and desertification. *J. Theor. Biol.* **2009**, *261*, 194–209.
30. Klausmeier, C.A. Regular and Irregular Patterns in Semiarid Vegetation. *Science* **1999**, *284*, 1826–1828.
31. Rietkerk, M.; Boerlijst, M.C.; van Langevelde, F.; HilleRisLambers, R.; van de Koppel, J.; Kumar, L.; Prins, H.H.T.; de Roos, A.M. Self-organization of vegetation in arid ecosystems. *Am. Nat.* **2002**, *160*, 524–530.
32. Sheffer, E.; von Hardenberg, J.; Yizhaq, H.; Shachak, M.; Meron, E. Emerged or imposed: a theory on the role of physical templates and self-organisation for vegetation patchiness. *Ecol. Lett.* **2012**, *16*, 127–139.
33. Yizhaq, H.; Sela, S.; Svoray, T.; Assouline, S.; Bel, G. Effects of heterogeneous soil-water diffusivity on vegetation pattern formation. *Water Resour. Res.* **2014**, *50*, 5743–5758.
34. Chesson, P.; Gebauer, R.L.E.; Schwinning, S.; Huntly, N.; Wiegand, K.; Ernest, M.S.K.; Sher, A.; Novoplansky, A.; Weltzin, J.F. Resource pulses, species interactions, and diversity maintenance in arid and semi-arid environments. *Oecologia* **2004**, *141*, 236–253.
35. Ursino, N.; Contarini, S. Stability of banded vegetation patterns under seasonal rainfall and limited soil moisture storage capacity. *Adv. Water Resour.* **2006**, *29*, 1556–1564.
36. Guttal, V.; Jayaprakash, C. Self-organization and productivity in semi-arid ecosystems: Implications of seasonality in rainfall. *J. Theor. Biol.* **2007**, *248*, 490–500.
37. Aguilar, E.; Barry, A.A.; Brunet, M.; Ekang, L.; Fernandes, A.; Massoukina, M.; Mbah, J.; Mhanda, A.; do Nascimento, D.J.; Peterson, T.C.; et al. Changes in temperature and precipitation extremes in western central Africa, Guinea Conakry, and Zimbabwe, 1955–2006. *J. Geophys. Res.* **2009**, *114*, D02115.
38. Leauthaud, C.; Demarty, J.; Cappelaere, B.; Grippa, M.; Kergoat, L.; Velluet, C.; Guichard, F.; Mougin, E.; Chelbi, S.; Sultan, B. Revisiting historical climatic signals to better explore the future: Prospects of water cycle changes in Central Sahel. *Proc. Int. Assoc. Hydrol. Sci.* **2015**, *371*, 195–201.
39. Millennium Ecosystems Assessment. *Ecosystems and Human Well-Being: Desertification Synthesis*; World Resources Institute: Washington, DC, USA, 2005.
40. Siteur, K.; Siero, E.; Eppinga, M.B.; Rademacher, J.D.; Doelman, A.; Rietkerk, M. Beyond Turing: The response of patterned ecosystems to environmental change. *Ecol. Complex.* **2014**, *20*, 81–96.
41. Malchow, H.; Petrovskii, S.V.; Venturino, E. *Spatiotemporal Patterns in Ecology and Epidemiology: Theory, Models, and Simulation*; Mathematical and Computational Biology, Chapman and Hall/CRC: Boca Raton, FL, USA, 2008.
42. Rovinsky, A.B.; Menzinger, M. Chemical instability induced by a differential flow. *Phys. Rev. Lett.* **1992**, *69*, 1193–1196.
43. Siero, E.; Doelman, A.; Eppinga, M.B.; Rademacher, J.D.M.; Rietkerk, M.; Siteur, K. Striped pattern selection by advective reaction-diffusion systems: Resilience of banded vegetation on slopes. *Chaos* **2015**, *25*, 036411.
44. Sherratt, J.A. An analysis of vegetation stripe formation in semi-arid landscapes. *J. Math. Biol.* **2005**, *51*, 183–197.
45. Sherratt, J.A. Pattern solutions of the Klausmeier model for banded vegetation in semi-arid environments II: Patterns with the largest possible propagation speeds. *R. Soc. A* **2011**, *467*, 3272–3294.
46. Siekmann, I.; Malchow, H. Fighting enemies and noise: Competition of residents and invaders in a stochastically fluctuating environment. *Math. Model. Nat. Phenom.* **2016**, *11*, 120–140.
47. Maruyama, G. Continuous Markov processes and stochastic equations. *Rend. Circ. Mat. Palermo* **1955**, *4*, 48–90.
48. MATLAB: Version 8.1 (R2013a); The MathWorks Inc.: Natick, MA, USA, 2013.
49. Ermentrout, B. *Simulating, Analyzing, and Animating Dynamical Systems: A Guide to Xppaut for Researchers and Students*; Society for Industrial and Applied Mathematics: Philadelphia, PA, USA, 2002.
50. Tantau, T. The TikZ and PGF Packages. Manual for Version 3.0.1. Available online: http://sourceforge.net/projects/pgf/ (accessed on 6 July 2017).
51. Sherratt, J.A.; Lord, G.J. Nonlinear dynamics and pattern bifurcations in a model for vegetation stripes in semi-arid environments. *Theor. Popul. Biol.* **2007**, *71*, 1–11.
52. Deutscher Wetterdienst. Klimatafel von Niamey (Aéro)/Niger (In German). Available online: http://www.dwd.de/DWD/klima/beratung/ak/ak_610520_kt.pdf (accessed on 15 April 2017).